ACADEMIC PRESS

Available online at www.sciencedirect.com

SCIENCE DIRECT®

Journal of Sound and Vibration 261 (2003) 93–107

JOURNAL OF SOUND AND VIBRATION

www.elsevier.com/locate/jsvi

Modelling and characterization of a piezoceramic inertial actuator

G.A. Lesieutre[a], R. Rusovici[b,*], G.H. Koopmann[c], J.J. Dosch[d]

[a] *Department of Aerospace Engineering, The Pennsylvania State University, University Park, PA 16802, USA*
[b] *STI Technologies Inc., PCB Group, 1800 Brighton-Henrietta Townline Rd., Rochester, NY 14623, USA*
[c] *Department of Mechanical Engineering, The Pennsylvania State University, University Park, PA 16802, USA*
[d] *PCB Piezotronics Inc., Depew, NY 14043, USA*

Received 2 July 2001; accepted 29 April 2002

Abstract

An inertial actuator (also known as a proof mass actuator) applies forces to a structure by reacting them against an "external" mass. This approach to actuation may provide some practical benefits in the active control of vibration and structure-borne noise: system reliability may be improved by removing the actuator from a structural load path; effective discrete point-force actuation permits ready attachment to curved surfaces, and an inherent passive vibration absorber effect can reduce power requirements.

This paper describes a class of recently developed inertial actuators that is based on mechanical amplification of displacements of an active piezoceramic element. Important actuator characteristics include resonance frequencies, clamped force, and the drive voltage to output the force frequency response function.

The paper addresses one particular approach to motion amplification, the "dual unimorph," in detail. A model of actuator dynamic behavior is developed using an assumed-modes method, treating the piezoelectrically induced stresses as external forces. Predicted actuator characteristics agree well with experimental data obtained for a prototype actuator. The validated actuator dynamic model provides a tool for design improvement.

1. Introduction

Active control technology has potential applications to many noise and vibration problems, including aircraft cabin interior noise, spacecraft vibration suppression, and automobile,

*Corresponding author. Tel.: +585-424-2010; fax: +585-272-7201.
E-mail address: rrusovici@yahoo.com (R. Rusovici).

0022-460X/03/$ - see front matter
PII: S0022-460X(02)00943-4

industrial machinery and home appliances [1–5]. Practical deployment of this technology requires, among other things, the development of light, efficient, reliable, cost-effective actuators.

Moving coil electrodynamic devices are inherently capable of large displacements and have been widely used as the basis for inertial actuators [6–8]. Initial research by the authors had indicated the potential for piezoceramic inertial actuators to provide higher power density, better linearity and decreased power consumption, especially for moderately high frequency (100–10,000 Hz) applications [9].

The purpose of the research described herein was to explore the potential performance of piezoceramic inertial actuators in more detail. Both analytical and experimental aspects were addressed.

2. Piezoceramic inertial actuator concepts

Piezoelectric materials have found wide use in inertial sensor (e.g., accelerometer) applications because of high electromechanical transduction properties. These properties also make such materials excellent candidates for use in actuators. The need for rapid, high force linear response effectively limits the materials choice to piezoceramics [10].

An inertial actuator can be thought of as applying forces to a structure that are reacted by accelerating a supported mass. Even though piezoceramic materials are capable of providing high forces, there has been little prior development of inertial actuators using them, largely because of the small strains (displacements) developed and high inherent stiffness. Both of these factors limit the practical performance achievable using direct piezoelectric acceleration of a given mass in the frequency range of interest.

The development and use of mechanical amplification methods is essential to the practical success of piezoceramic inertial actuation. Several approaches to mechanical amplification [11–15] were explored in this research. Fig. 1 shows schematically three of the general concepts considered. For purposes of discussion, these may be considered to be either planar or axisymmetric.

In the "lever" concept, the expansion of a piezoelectric element is mechanically amplified through a hinged linkage to produce larger motions of the attached mass.

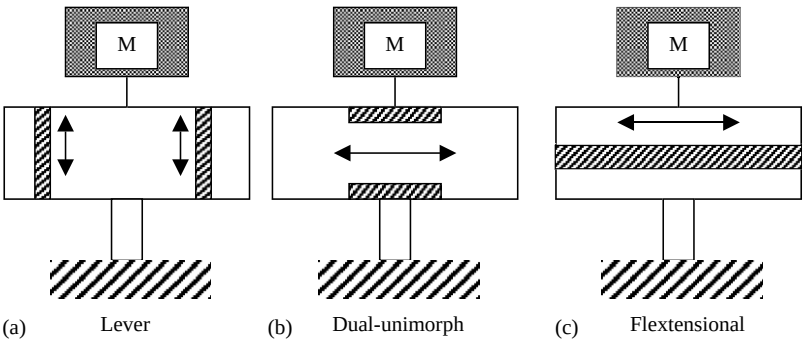

Fig. 1. Three concepts for mechanical amplification of piezoceramic displacement in an inertial actuator. (a) lever, (b) dual-unimorph, (c) flextensional.

In the "dual unimorph" concept, thin piezoceramic layers are attached to flat end caps. In-plane actuation of the piezoceramic bends the 2-layer composite plate and produces transverse motion of the attached mass. "Unimorph" actuation is a well-known means of obtaining displacement amplification.

In the "flextensional" concept, in-plane actuation of a piezoceramic layer produces in-plane motion of the edges of curved end caps. The curvature of the end caps produces transverse motion of the attached mass. "Flextensional" actuation is also a well-known means of obtaining displacement amplification.

It is not the purpose of this paper to compare the relative merits of these three motion amplification concepts for application to inertial actuators. Instead, one of the concepts is chosen and used as the focus for the development of a general modelling approach and its experimental validation. Due to its relative simplicity, the "dual unimorph" concept was chosen for evaluation.

Note that any of these approaches will have the following general qualitative effects in comparison to direct piezoelectric motion of a given mass: (1) larger displacement and higher force output at low (quasistatic) frequencies; (2) lower natural frequencies of vibration; and (3) lower clamped force (defined when the mass is prevented from moving). The quantitative effects depend on the motion amplification factor, as well as the actuator structural stiffnesses (series and parallel) relative to the piezoceramic stiffness [1,6].

3. Dual unimorph piezoceramic inertial actuator model

A model of the dynamic behavior of a dual unimorph piezoceramic inertial actuator is developed using an assumed modes method. An approximate numerical approach such as this is appropriate because of the geometric complexity of the actuator depicted in Fig. 2.

Key aspects of the analysis approach include the following: (1) the actuator is assumed to be driven by voltage signal; (2) the piezoceramic material stiffness (at constant electrical field) is

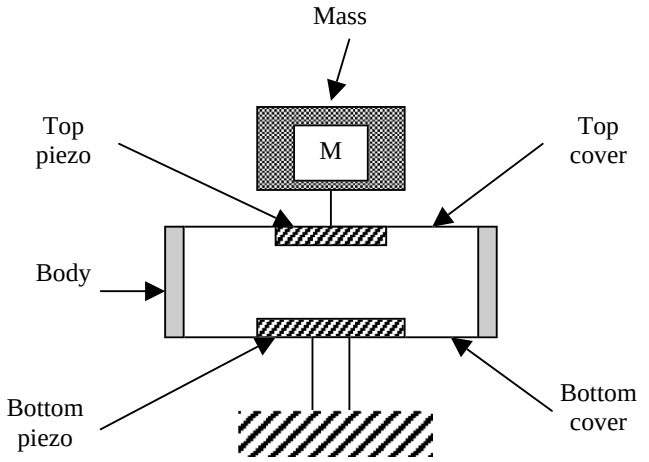

Fig. 2. Dual unimorph actuator geometry.

included in the development of an elastic model of the actuator: and the piezoelectrically induced stresses (at zero strain) are treated as external forces.

An important output from the model is a predicted frequency response function from the actuator drive voltage signal to the output force for the situation in which the actuator is attached to a rigid structure. Such a frequency response function can be readily determined in the laboratory for comparison. Other important outputs available from the model include natural vibration frequencies and clamped force; these may also be determined approximately from the frequency response function.

3.1. Geometry, key features, and assumptions

In the model developed, the following geometrical, material, and physical parameters completely characterize an actuator design: actuator radius, a; top cover thickness, h_{ct}; bottom cover thickness, h_{cb}, cover material (E_c, ν_c, ρ_c); top piezo radius and thickness, a_{pt} and h_{pt}; bottom piezo radius and thickness, a_{pb} and h_{pb}; piezo material (E_p, ν_p, d_{31}); cover-body joint stiffness, k_Θ; body mass, m_B; and attached reaction mass, m_R.

The top and bottom covers are assumed to have the same diameter ($2a$) and be made of the same isotropic material. The two covers are connected via the body, which is assumed to transmit vertical motion perfectly; i.e., the vertical displacement of the outer edges of both covers is assumed to be the same. Although the body is assumed to be rigid, it is not massless.

A "cover-body joint stiffness" (or simply "joint stiffness") is introduced to allow non-zero cover radial rotation at the joint with the rigid body. If the joint stiffness is very small, the cover is essentially simply supported; if the joint stiffness is very large, the cover is essentially clamped. The stiffness of this welded or bonded joint is very difficult to estimate accurately a priori and provides a single parameter that may be adjusted to improve the agreement of model predictions with experimental data.

The top and bottom covers are allowed to have different thicknesses. In addition, the top and bottom piezoceramic layers may have different diameters as well as different thicknesses.

The top and bottom piezoceramic layers are made of the same material, assumed to be poled and driven in the thickness ("3") direction. Since common PZT materials are isotropic in the 1–2 plane, an effective isotropic Young's modulus and the poisson ratio may be defined; these assume plane stress and constant electrical field conditions [17]. In addition, since the important mode of piezoelectric actuation is in the 1–2 plane for an electrical field in the 3 direction, only the piezoelectric coupling property d_{31} is of consequence.

Furthermore, each cover–piezoceramic combination (top and bottom) is assumed to behave as an axisymmetric perfectly bonded composite plate in accordance with Kirchoff plate theory [18]. Normal radial and tangential strains (ε_{rr}, $\varepsilon_{\theta\theta}$) are assumed to vary linearly with distance from the modulus-weighted midplane; midplane strains are taken to be zero. A slight complication of allowing a piezoceramic layer to have a diameter different from the actuator diameter is that the modulus-weighted midplane of the composite (multi-component) plate is discontinuous.

3.2. Assumed modes model

As noted in the preceding section, the geometric complexity of the actuator motivates the development of an approximate numerical model. In prior work, an actuator concept based on flextensional displacement amplification was modelled using finite elements [16]. While a detailed FE model of a dual unimorph actuator could be readily constructed (some commercial FE codes offer piezoelectric elements), such a model can be cumbersome for use in preliminary design and sizing.

Because of the radial symmetry of the actuator concept considered, the possibility of developing a low order model with the ability to accurately predict important first order actuator performance characteristics seemed good and was pursued.

This low order model was based on the method of assumed modes with non-conservative forcing [19]. This method is basically an energy approach in which the physical displacements of a structure are represented as a sum of analyst-defined displacement shape functions scaled by time-dependent coefficients (or generalized co-ordinates). The resulting mathematical model is a set of ODEs in the generalized co-ordinates.

3.2.1. Assummed modes (shape functions)

In this model, the overall displacements of the actuator are represented conceptually as a combination of displacements of the bottom cover and the top cover. The displacement approximation chosen must satisfy all the geometric boundary conditions of the problem.

An initial model may be developed by assuming that the center of the bottom cover is fixed. The force between the actuator and the structure may be found by permitting motion of this point, then finding the force required preventing such motion. The transverse displacement of the bottom plate midplane, $w_b(r,t)$, may be approximated as

$$w_b(r,t) = \sum_{i=1}^{n} W_{bi}(r)c_i(t), \tag{1}$$

where the $W_b(r)$ are the assumed modes and the $c_i(t)$ are the generalized co-ordinates for the bottom plate. The assumed modes must satisfy the following geometric conditions:

$$\begin{aligned} &W_{bi}(r=0) = 0, \quad \text{zero displacement;} \\ &\frac{\partial W_{bi}}{\partial r}(r=0) = 0, \quad \text{zero slope (symmetry).} \end{aligned} \tag{2}$$

In addition, it will be convenient to have

$$W_{bi}(r=a) = 1, \tag{3}$$

as this gives the c_i a physical interpretation as the transverse displacements at the edge of the bottom plate associated with assumed mode i.

Note that all that is needed to allow motion at the center of the bottom cover is to introduce an additional coefficient $c_0(t)$ with a unity shape function $W_{b0}(r) = 1$; c_0 is just the displacement at this point.

There are at least two ways to accommodate the effects of imperfect rotational continuity between the body and covers (joint stiffness). The first is to choose the assumed modes so that

they explicitly satisfy the mixed moment-slope boundary condition at the cover edge (r = a): a restoring moment (per unit length) is proportional to the angular deflection (radial slope). The second is to assume a simply supported (geometric) boundary, and to include the effects of the joint stiffness in the expression for the system potential energy.

The first way has the advantage of using "higher quality" assumed modes, while the second has the advantage of allowing more ready consideration of the effects of joint damping. Both ways were implemented in this work and were found to give comparable results using a few degrees of freedom.

The following polynomial form for the assumed modes satisfies the required boundary conditions:

$$W_{bi}(r) = A_i\left(\frac{r}{a}\right)^{i+2} + B_i\left(\frac{r}{a}\right)^{i+4}, \tag{4}$$

where

$$A_i = \frac{(i+4) + (i+4)(i+3)\left(D_{cb}/ak_\theta\right)}{2 + (4i+10)\left(D_{cb}/ak_\theta\right)}, \quad B_i = 1 - A_i, \tag{5}$$

and D_{cb} is the bottom cover flexural rigidity:

$$D_{cb} = \frac{E_c h_{cb}^3}{12(1-\upsilon_c^2)}. \tag{6}$$

Now, the transverse displacement of the top plate midplane, $w_t(r,t)$ may be approximated as

$$w_t(r,t) = \sum_{i=1}^{n} c_i(t) + \sum_{j=1}^{n}(1 - W_{tj}(r))d_j(t), \tag{7}$$

where the $d_j(t)$ are the generalized co-ordinates for the top, and the same number of assumed modes, n, are used to represent deformation of the top plate as the bottom. Note that the $W_{tj}(r)$ functions that appear in this expression are similar to the $W_{bi}(r)$ that comprise the assumed modes for the bottom plate; the difference being in the possibility that D_{ct} is different from D_{cb}.

Note that this expression satisfies the following geometric conditions:

$$\begin{aligned} &w_t(r=a,t) = w_b(r=a,t), && \text{edge displacement,}\\ &\frac{\partial w_t}{\partial r}(r=0,t) = 0, && \text{slope (symmetry),} \end{aligned} \tag{8}$$

and for convenience:

$$w_t(r=0,t) = \sum_{i=1}^{n} c_{\mathrm{i}}(\mathrm{t}) + \sum_{j=1}^{n} d_{\mathrm{j}}(t). \tag{9}$$

In addition, if the coefficients A_j and B_j are selected as described in the preceding Eq. (5), the assumed modes for the top plate will also explicitly satisfy the mixed moment–slope boundary condition.

3.2.2. Mass matrix development

The model mass matrix may be found by expressing the kinetic energy of the actuator in terms of the time derivatives of the generalized co-ordinates of the model.

The total kinetic energy of the actuator is given as the sum of the kinetic energies of its parts: (1) the top plate; (2) the bottom plate; (3) the body mass; and (4) the reaction mass.

The kinetic energy for the plate parts of the actuator has the form

$$T^* = \frac{1}{2}(2\pi)\int_0^a \rho^* h^* \left(\frac{\partial w^*}{\partial r}\right)^2 r\,\mathrm{d}r, \tag{10}$$

where $\rho^* h^*$ is the total mass density per unit area. Note that if the piezoceramic radius is less than the actuator radius, $\rho^* h^*$ is not constant in this integral.

The expressions in the preceding Eqs. (8) and (9) for $w_b(r,t)$ and $W_t(r,t)$ may be used to determine the individual contributions of the top and bottom plates to the actuator mass matrix.

The body mass kinetic energy is given by

$$T_B = \frac{1}{2} m_B \left(\frac{\partial w_b(r=a,t)}{\partial t}\right)^2, \tag{11}$$

and the kinetic energy of the reaction mass by

$$T_R = \frac{1}{2} m_R \left(\frac{\partial w_t(r=0,t)}{\partial t}\right)^2. \tag{12}$$

The total actuator kinetic energy may be expressed in matrix form in terms of the mass matrix and the generalized velocities as

$$T_R = \frac{1}{2}\left\{\begin{matrix}\dot{c}\\ \dot{d}\end{matrix}\right\}^T [M] \left\{\begin{matrix}\dot{c}\\ \dot{d}\end{matrix}\right\}. \tag{13}$$

3.2.3. Stiffness matrix development

The model stiffness matrix may be found by expressing the strain energy of the actuator in terms of the generalized co-ordinates of the model.

The total strain energy of the actuator is given as the sum of the strain energies of its parts: (1) the top plate; (2) the bottom plate; and, if the simply supported assumed modes are being used, (3) the body-cover joint.

The strain energy for the plate parts of the actuator has the form

$$U^* = \frac{1}{2}(2\pi)\int_0^a D^* \left[\left(\frac{\partial^2 w^*}{\partial r^2} + \frac{1}{r}\frac{\partial w^*}{\partial r}\right)^2 - 2(1-\nu^*)\frac{\partial^2 w^*}{\partial r^2}\left(\frac{1}{r}\frac{\partial w^*}{\partial r}\right)\right] r\,\mathrm{d}r, \tag{14}$$

or

$$U^* = \pi\int_0^a D^* \left\{\begin{matrix}\dfrac{\partial^2 w^*}{\partial r^2}\\ \dfrac{\partial w^*}{\partial r}\end{matrix}\right\}^T \left[\begin{matrix}1 & \dfrac{\nu^*}{r}\\ \dfrac{\nu^*}{r} & \dfrac{1}{r^2}\end{matrix}\right] \left\{\begin{matrix}\dfrac{\partial^2 w^*}{\partial r^2}\\ \dfrac{\partial w^*}{\partial r}\end{matrix}\right\} r\,\mathrm{d}r. \tag{15}$$

Note that if the piezoceramic radius is less than the plate radius, the flexural rigidity D^* is not constant in this integral. In addition, as noted in the preceding section, the modulus-weighted midplane will generally be discontinuous, which must also be accounted for. In regions of a plate that have both a cover and piezoceramic parts, the effective composite flexural rigidity depends on component material moduli, the Poisson ratios, thicknesses, and relative stiffness and thickness.

If it is to be explicitly included (not implicitly in the shape functions used), the strain energy of the body-cover joint stiffness is given by

$$U^* = \frac{1}{2}(2\pi)k_\theta \left(\frac{\partial w^*(r=a,t)}{\partial r} \right)^2. \tag{16}$$

Note that the individual contributions of the joint stiffnesses for both the top and bottom body-cover joints must be included. The joint stiffness contains an imaginary term (damping), due to the presence of a layer of high-damping material at the joint

The total actuator strain energy may be expressed in matrix form in terms of the model stiffness matrix and the generalized co-ordinates as

$$U = \frac{1}{2} \left\{ \begin{array}{c} c \\ d \end{array} \right\}^T [K] \left\{ \begin{array}{c} c \\ d \end{array} \right\}. \tag{17}$$

3.2.4. Piezoelectric force vector development

The model force vector may be found by expressing the virtual work done by the "piezoelectric" stresses (clamped, at constant strain) in terms of the generalized co-ordinates of the model. Note that the equivalent of the virtual work of the "elastic" stresses has been included in the strain energy.

The virtual work of the piezoelectric stresses acting on plate is given approximately by

$$\delta W^* = 2\pi h_{p^*} \int_0^{a_{p^*}} (\sigma_{rr}\delta\varepsilon_{rr} + \sigma_{\theta\theta}\delta\varepsilon_{\theta\theta}) r \, \mathrm{d}r, \tag{18}$$

where the stresses and virtual strains are defined at the geometric midplane of the (thin) piezoceramic layer in terms of the assumed modes.

The piezoelectric clamped stresses are found from the piezoceramic material constitutive equations as

$$\sigma_{\theta\theta} = \sigma_{rr} = -\frac{E_p}{(1-\upsilon_p)} d_{31} \frac{V}{h_{p^*}}. \tag{19}$$

Note that these clamped stresses are equal; as noted in the preceding Eq. (19), the material is isotropic in the plane transverse to the poling direction. In addition, note that the quantity V/h_{p^*} is the strength of the applied electrical field (decreasing electrical potential in the positive 3 (z) direction is a positive electric field). Care must be taken to ensure that the correct sign of this field is used for the top and bottom plate parts.

The strain–displacement relations may be used to express the virtual strains in terms of the transverse displacements (and the generalized co-ordinates) as

$$\varepsilon_{rr} = \frac{\partial u_r}{\partial r} = -z_{p^*}\frac{\partial^2 w^*}{\partial r^2}, \quad \varepsilon_{\theta\theta} = \frac{1}{r}\frac{\partial u_\theta}{\partial r} + \frac{1}{r}u_r = -\frac{z_{p^*}}{r}\frac{\partial w^*}{\partial r}, \tag{20}$$

where z_{p^*} is the distance from the modulus-weighted composite midplane to the piezoceramic geometric midplane.

The virtual work expression then becomes

$$\delta W^* = 2\pi h_{p^*}\int_0^{a_{p^*}} \frac{E_p}{(1-\upsilon_p)} d_{31}\frac{V}{h_{p^*}}\delta\left(z_{p^*}\frac{\partial^2 w^*}{\partial r^2} + \frac{z_{p^*}}{r}\frac{\partial w^*}{\partial r}\right) r\,\mathrm{d}r \tag{21}$$

or

$$\delta W^* = 2\pi\frac{E_p V}{(1-\upsilon_p)} d_{31} z_{p^*}\int_0^{a_{p^*}} \delta\left(\frac{\partial^2 w^*}{\partial r^2} + \frac{1}{r}\frac{\partial w^*}{\partial r}\right) r\,\mathrm{d}r \tag{22}$$

Note that the contributions of both the top and bottom piezoceramic elements must be included.

The total virtual work of the piezoelectric clamped stresses may then be expressed in matrix form in terms of the generalized co-ordinates and the generalized force vector as

$$\delta W = \begin{Bmatrix} c \\ d \end{Bmatrix}^T \begin{Bmatrix} f_c \\ f_d \end{Bmatrix} V(t). \tag{23}$$

3.2.5. Actuator dynamic equations

Using the preceding results for kinetic energy, strain energy, and virtual work, the matrix ODE that govern the dynamic response of the actuator are found as:

$$[M]\begin{Bmatrix} \ddot{c} \\ \ddot{d} \end{Bmatrix} + [K]\begin{Bmatrix} c \\ d \end{Bmatrix} = \begin{Bmatrix} f_c \\ f_d \end{Bmatrix} V(t). \tag{24}$$

As noted in the previous discussion of assumed modes options, one approach to including damping would be to allow the body-cover stiffness to be complex. This approach yields a complex stiffness matrix $[K]$, and is most suitable for frequency-domain response analyses.

These equations, especially when augmented with a generalized co-ordinate corresponding to the base displacement, provide a means for rapid numerical exploration of actuator performance.

The equation for the fixed base force has the general form

$$F = \begin{Bmatrix} m_c \\ m_d \end{Bmatrix}^T \begin{Bmatrix} \ddot{c} \\ \ddot{d} \end{Bmatrix}. \tag{25}$$

Note that the actuator is incapable of applying a static force at its base because no mass is accelerated.

3.3. Predicted actuator performance

Of special interest is the predicted frequency response function from the actuator drive voltage signal to the output force for the situation in which the actuator is attached to a rigid structure. Other important outputs available from the model include natural vibration frequencies and clamped force.

3.3.1. Natural modes of vibration

To determine the natural modes of vibration, an eigenvalue problem corresponding to the unforced dynamics equations is solved. This problem has the form

$$\left[[K] - \omega^2[M]\right] \left\{ \begin{array}{c} c \\ d \end{array} \right\}_n = \left\{ \begin{array}{c} 0 \\ 0 \end{array} \right\}, \tag{26}$$

where ω_n is the natural frequency of vibration mode n, and $\{cd\}_n T$ is the corresponding eigenvector. The approximate mode shape is then found as a sum of the assumed modes, each weighted by the corresponding coefficient (generalized displacement).

Note that these equations correspond to the case in which the electrical field across the piezoelectric layers is constant. This is usually accomplished by connecting the leads together, and causes the material to behave with its short-circuit stiffness, Ep.

3.3.2. Clamped force

This performance measure is just the force at the actuator base when both the base and the reaction mass are prevented from moving when a drive signal is applied. It is commonly described in terms of output force per input voltage. The clamped force is a useful quantity because it corresponds to the situation in which the actuator can react the structural force against an unmoving reference point. For typical actuator designs considered, this situation is nearly encountered at a forcing frequency in between the first and second natural frequencies of vibration. In practice, an actuator can deliver higher forces, especially at frequencies near resonance.

3.3.3. Frequency response

To determine the frequency response function (FRF) of an actuator design from the model, the following problem is addressed. A harmonic drive voltage is applied to the actuator, and the resulting, steady state response at the drive frequency is determined. The magnitude (force/volt) and phase (degrees) of the ratio of the output force to the drive voltage is recorded for comparison to experimental data.

First, the following equation is solved for the complex generalized co-ordinates at a specified forcing frequency, ω

$$\left[[K] - \omega^2[M]\right] \left\{ \begin{array}{c} c \\ d \end{array} \right\} e^{i\omega t} = \left\{ \begin{array}{c} f_c \\ f_d \end{array} \right\} V_0 e^{i\omega t}. \tag{27}$$

Then, the fixed base force is found using:

$$F_0 = -\omega^2 \begin{Bmatrix} m_c \\ m_d \end{Bmatrix}^T \begin{Bmatrix} c \\ d \end{Bmatrix}. \tag{28}$$

The value of the frequency response function at the forcing frequency is just the ratio of F_0 to V_0. To generate a frequency response plot, this procedure is repeated at a number of forcing frequencies over the range of interest.

4. Actuator experimental characterization

A prototype dual-unimorph actuator was fabricated at PCB Piezotronics for evaluation purposes. This actuator was tested by simulating a fixed base condition in the laboratory, as illustrated in Fig. 3.

The actuator was attached to a very large base mass through a stiff force transducer. It was driven by a prescribed voltage signal and the output force signal measured using the force transducer. The frequency response function over a range of interest was determined either by sweeping slowly through the range, or by using FFT methods. Both approaches gave comparable results.

5. Results

Fig. 4 shows predicted frequency response results (magnitude only) for a nominal actuator design (the tested prototype). These results were obtained using 11 assumed modes in the displacement approximations for each of the top and bottom plates. Three responses are shown, corresponding to simply supported, clamped, and intermediate (between simply supported and clamped) values of the joint stiffness (with no damping). Modal frequencies increase with increasing stiffness, as expected. The behavior of the actual joint is expected to lie between these extremes. The actuator is loaded with a 150-g inertial mass.

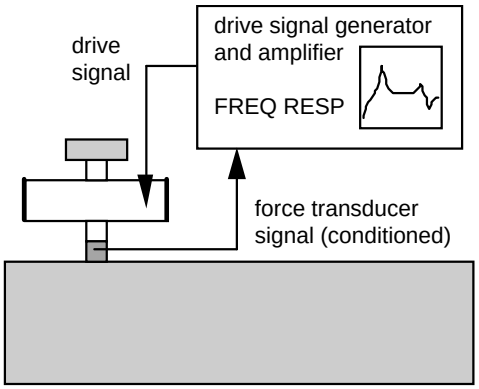

Fig. 3. Laboratory setup for actuator characterization.

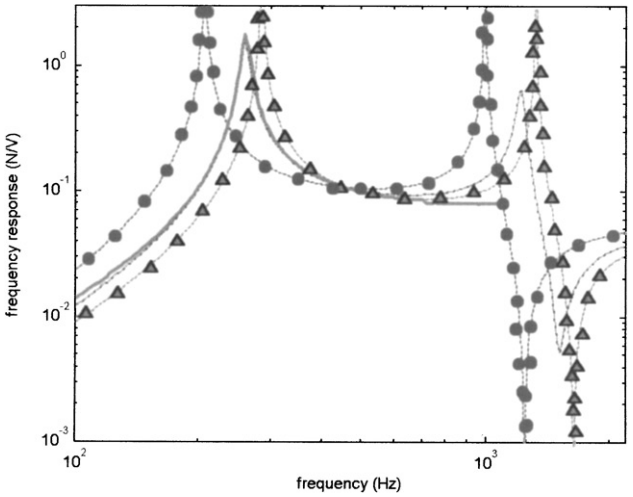

Fig. 4. Predicted FRFs for prototype actuator with extreme (and no damping) and intermediate joint stiffnesses (150 g mass): ●, simply supported; ▲, clamped, — prediction w/150 g mass; —, experiment w/150 g mass.

Table 1
Model geometric input parameters for baseline actuator

a (mm)	h_{ct} (mm)	h_{cb} (mm)	a_{pt} (mm)	h_{pt} (mm)	a_{pb} (mm)	h_{pb} (mm)
20	0.6	0.6	16.5	0.5	16.5	0.5

Table 2
Model material input parameters for baseline actuator

s_{11} (m^2/N)	s_{12} (m^2/N)	d_{31} (pC/N)	k_θ (N)	m_R (g)	E_c (Pa)	v_c
16.2e−12	−4.54e−12	−220	1300 + j*450	25	1.14e + 11	0.32

Notice the relatively flat range in the frequency response function between the first and second axisymmetric natural frequencies. In this range, the force level is very nearly (actually slightly greater than) the clamped force. This may be understood by considering the nature of the first two modes. In the first mode, the body mass and the reaction mass move together; in the second mode, the body mass and the reaction mass move in opposition. As the frequency increases through this range, the reaction mass is nearly still, acting almost as a hard reference point against which to push and pull. Input geometry parameters and input material properties used in calculations are shown in Tables 1 and 2, respectively.

Fig. 5 shows several predicted actuator frequency response function magnitudes against corresponding experimental data, for three different values of the reaction mass.

Damping was included in the predictions by allowing the body-cover joint stiffness to be complex; the same (complex) joint stiffness was used in all predictions.

The predicted behavior agrees well with the experimental results in terms of natural frequencies, damping, and the force level over the frequency range between the first and second natural

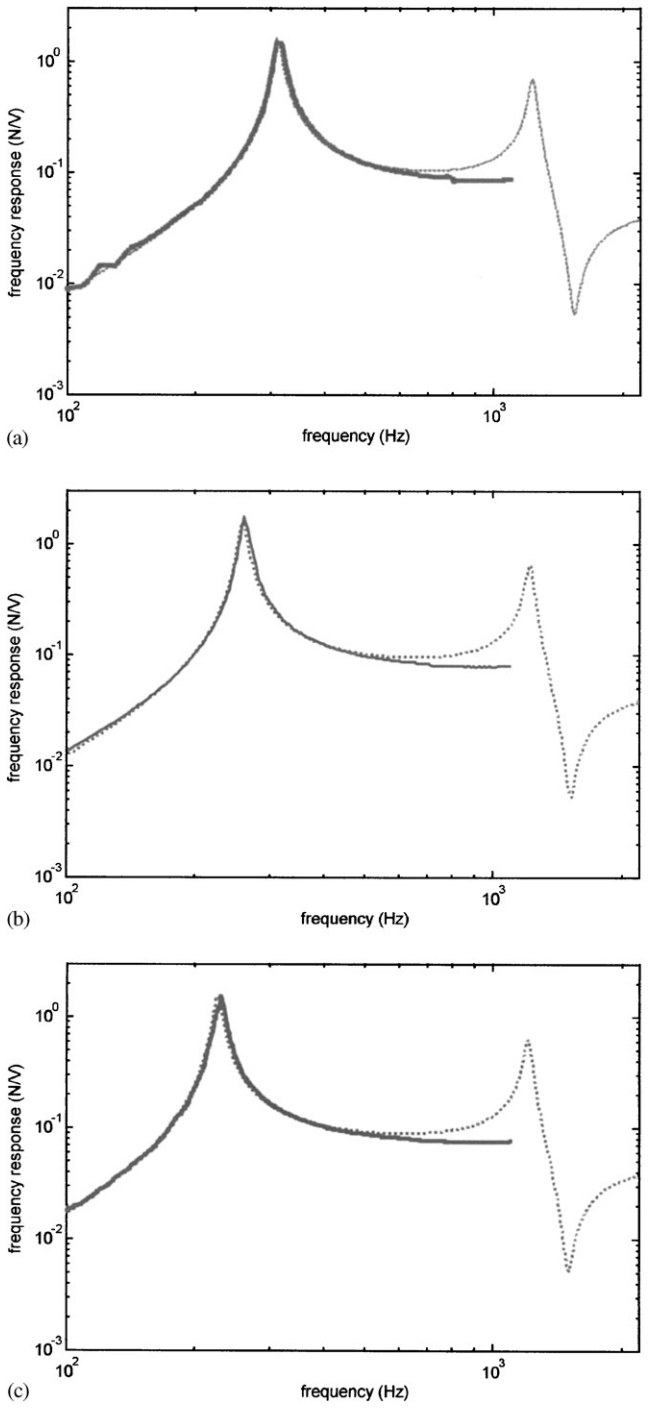

Fig. 5. Comparison of predicted and experimental FRFs for prototype actuator, with changing reaction mass: (a) —, 100 g-predicted, —, 100 g-experiment; (b) —, 150 g-predicted, —, 150 g-experiment; (c) —, 200 g-predicted, —, 200 g-experiment.

Table 3
Comparison of predicted to experimental data [20]

Parameter	$f1$ (Hz)	$f2$ (Hz)	Blocked force (N)
Predicted	267	1289	0.0675
Experimental	260	1250	0.067
% Error	$<3\%$	3%	$<1\%$

Fig. 6. 712 series dual-unimorph piezoceramic actuator manufactured by PCB Piezotronics Inc. Photo courtesy of PCB Piezotronics Inc., published with permission [20].

frequencies. Table 3 shows a comparison of the predicted and experimental natural frequencies and blocked force level for a baseline actuator loaded with a 150-g mass.

Considering that the predictions were attained using just 10 degrees of freedom and a single adjustable parameter (the joint stiffness), the agreement is quite satisfactory.

6. Summary

A light, efficient, reliable, cost-effective actuator might find near-term use in active noise and vibration control applications. Initial analytical and experimental research has explored the potential performance of a piezoceramic inertial actuator with mechanical amplification. Several concepts for mechanical amplification were considered, including "lever," "dual unimorph," and "flextensional."

A low-order model of a "dual unimorph" actuator concept was developed using the method of assumed modes. Composite plates comprised of a metal cover with an attached active piezoceramic layer were assumed to behave in a manner consistent with the kinematic assumptions of Kirchoff plate theory. The short-circuit stiffness of the piezoceramic material was included in the development of the elastic part of the model, while the piezoelectric (clamped) stresses were used in the development of the forcing terms. A key aspect of the model was the use of assumed modes that explicitly satisfied a mixed moment-slope boundary condition due to a presumed body-cover joint stiffness.

A prototype actuator was built and characterized experimentally. Measures of performance included resonance frequencies, clamped force, and voltage-to-force frequency response.

The low-order model accurately captured the key features of measured actuator performance. The model was used to gain additional insight into the physical behavior of piezoceramic inertial actuators and in developing guiding potential design modifications. The results of this research were used to develop the commercially available 712 PCB Piezotronics Inc. series of dual-unimorph piezoceramic actuators, shown in Fig. 6.

Acknowledgements

This research was supported by PCB Piezotronics, Inc. and NASA under SBIR contract NAS 1-20205.

References

[1] R.J. Silcox, Mechanisms of active control in cylindrical fuselage structures, American Institute of Aeronautical and Astronautics Journal 28 (8) (1990) 1397–1404.
[2] C.R. Fuller, Active control of interior noise in model aircraft fuselages using piezoceramic actuators, American Institute of Aeronautical and Astronautics Journal 30 (I1) (1992) 2613–2617.
[3] H. Ulbrich, Elements of active vibration control for rotating machinery, NASA Technical Memorandum 102368 (1990) 48.
[4] R. Thomas, Active control of fan noise from a turbofan engine, AIAA Journal 32 (1) (1994) 23–30.
[5] P.A. Nelson, S.J. Elliott, Active Control of Sound, Academic Press Ltd., London, 1992.
[6] D.W. Miller, E.F. Crawley, Theoretical and experimental investigation of space-realizable inertial actuation for passive and active structural control, Journal of Guidance, Control, and Dynamics Volume 11 (5) (1988) 449–458.
[7] G.L. Slater, S. Shelley, M. Jacobson, Analysis, design, and testing of a low-cost, direct force command, linear proof mass actuator for structural control, NASA CP-3177, Part 2, (1993) pp. 751–761.
[8] H.M. Macdonald, T.C. Green, B.W. Williams, Analysis and control of a moving coil electrodynamic actuator, IECON Proceedings (Industrial Electronics Conference) 3 (1993) 2184–2189.
[9] J.J. Dosch, G.A. Lesieutre, G.H. Koopmann, C.L. Davis, Inertial piezoceramic actuators for smart structures, Proceedings of the 1995 North American Conference on Smart Structures and Materials (SPIE Proceedings 2447) San Diego, CA, 26 February–3 March 1995.
[10] S. Yoshikawa,T.R. Shrout, multilayer piezoelectric actuators-structures and reliability, AIAA-93-171 I-CP, 1993, pp. 3581–3586.
[11] K.D. Rolt, History of the flextensional electroacoustic transducer, Journal of the Acoustical Society of America 87 (1990) 1340–1347.
[12] R.E. Newnham, Flextensional 'moonie' actuators, Proceedings of the IEEE Ultrasonics Symposium 1 (1993) 509–513.
[13] V.V. Varadan, L.C. Chin, V.K. Varadan, Finite-element modeling of flextensional electroacoustic transducers, Smart Materials and Structures 2 (4) (1993) 201.
[14] K-Y. Oh, Shape memory unimorph actuators using lead zirconate-based antiferroelectrics, Journal of the Ceramic Society of Japan 98 (8) (1990) 905–908.
[15] Y. Kondoh, Bimorph type actuators using lead zinc niobate-based ceramics, Japanese Journal of Applied Physics, Part 1: Regular Papers & Short Notes 30 (9B) (1991) 2260–2263.
[16] C.L. Davis, G.A. Lesieutre, Modeling piezoelectric flextensional inertial actuators, Final Report to PCB Piezotronics on Phase I SBIR project, September 1993.
[17] IEEE Standard on Piezoelectricity, ANSI/IEEE Std 176, 1987.
[18] A. Ugural, Stresses in Plates and Shells, McGraw-Hill, New York, 1981.
[19] L. Meirovitch, Computational Methods in Structural Dynamics, Sijthoff & Noordhoff, Rockville, MD, 1980.
[20] PCB Piezotronics Inc. 712 Series Piezoelectric Inertial Actuators with Damping Data Sheet, Depew, NY.